

# Prediction of Superconductivity at $\approx 30$ K in Compressed Body-Centered Cubic Yttrium

Prabhakar P. Singh\*

Department of Physics, Indian Institute of Technology, Powai, Mumbai- 400076, India

Using *ab initio* methods, we have studied the electron-phonon interaction in compressed, body-centered cubic (bcc) yttrium, which is predicted to be stable at 280 GPa [Melsen *et al*, Phys. Rev. B **48**, 15574 (1993)]. We find that compressed, bcc yttrium has a large electron-phonon coupling with  $\lambda = 1.8$ , leading to a superconducting transition temperature  $T_c \approx 30$  K or above. Our results indicate that the large electron-phonon coupling is due to the lattice hardening.

Recent experiments on pressure-induced increase in superconducting transition temperature  $T_c$  of yttrium [1] seem to suggest an almost continuous increase in  $T_c$  with pressure. With increase in pressure from ambient to 115 GPa, the structural changes [2, 3] in yttrium from hcp  $\rightarrow$  Sm-type  $\rightarrow$  dhcp  $\rightarrow$  trigonal are accompanied by increase in  $T_c$  from 6 mK [4] to 20 K [1]. In contrast,  $T_c$  increases with pressure only in the fcc phase of lithium as it changes from bcc  $\rightarrow$  fcc  $\rightarrow$  hR1  $\rightarrow$  cI16 with pressure going up to 70 GPa [5]. Thus, the pressure-induced changes in  $T_c$  seem to be intimately connected with the structural phase transitions in these metals [6].

It has been shown theoretically that yttrium would stabilize in a bcc phase above 280 GPa [7]. Taking a cue from the experiments on yttrium [1], it is not surprising to expect bcc yttrium to superconduct well above 20 K at pressures above 280 GPa. However, it is also possible that in this pressure range yttrium may start to behave like lithium [5, 8, 9, 10, 11].

To further investigate the changes in the superconducting properties of bcc yttrium, we have used density-functional-based methods to calculate its electronic structure, lattice-dynamical response and the electron-phonon interaction. Subsequently, we have solved the isotropic Eliashberg gap equation to obtain the superconducting transition temperature  $T_c$ .

Based on our calculations, we find that compressed, bcc yttrium has a large electron-phonon coupling with  $\lambda = 1.8$ , leading to a superconducting transition temperature  $T_c \approx 36$  K for  $\mu^* = 0.25$ . Such a large coupling is a direct consequence of lattice hardening and its subsequent coupling to Fermi electrons. We also find the electrons at Fermi energy to have predominantly  $t_{2g}$  symmetry. Before we describe our results, we briefly outline the computational details of our calculations. Further details can be found in our previous work [12] as well as the references therein. The notations used here are that of our previous work [12].

We have calculated the electronic structure, the phonon density of states,  $F(\omega)$ , and the Eliashberg function,  $\alpha^2F(\omega)$  of bcc yttrium using full-potential, linear muffin-tin orbital (LMTO) method [13, 14]. Subsequently, we have numerically solved the isotropic Eliashberg gap equation [15, 16, 17] for a range of  $\mu^*$  to obtain

the corresponding  $T_c$ .

The lattice constant  $a = 5.15$  a.u. used in our calculations for bcc yttrium approximately corresponds to a compressed volume equal to  $0.31v_0$ , where  $v_0$  is the experimentally determined equilibrium volume of hcp yttrium [2, 3, 12].

The charge self-consistent, full-potential, LMTO calculations for bcc yttrium was carried out with  $2\kappa$ -energy panel, 897  $\mathbf{k}$ -points in the irreducible wedge of the Brillouin zone, and the muffin-tin radius for yttrium was taken to be 2.22 atomic units. The  $4s$  state of yttrium was treated as a semicore state, while the  $4p$  state was treated as a valence state. The basis set used consisted of  $s$ ,  $p$ , and  $d$  orbitals at the yttrium site, and the potential and the wave function were expanded up to  $l_{max} = 6$ .

The Fermi surface, phonon density of states, and the Eliashberg function of bcc yttrium were calculated using the linear response code based on the full-potential, LMTO method. The Fermi surface was constructed using XCrySDen program [18] with eigenvalues calculated on a  $48 \times 48 \times 48$  grid in the reciprocal space. The dynamical matrices and the electron-phonon matrix elements were calculated on a  $8 \times 8 \times 8$  grid resulting in 29 irreducible  $\mathbf{q}$ -points. The Brillouin zone integrations during linear response calculations were carried out using a  $16 \times 16 \times 16$  grid of  $\mathbf{k}$ -points. The Fermi surface sampling for the evaluation of the electron-phonon matrix elements was done using a  $48 \times 48 \times 48$  grid. Another set of calculations of self-consistent charge density,  $F(\omega)$  and  $\alpha^2F(\omega)$  was carried out at a lattice constant  $a = 5.1987$  a.u. using a  $6 \times 6 \times 6$  grid with 16 irreducible  $\mathbf{q}$ -points. In this case, a  $12 \times 12 \times 12$  grid of  $\mathbf{k}$ -points was used for linear-response calculations, in conjunction with a  $36 \times 36 \times 36$  grid for Fermi surface sampling. The muffin-tin radius for yttrium was taken to be 2.251 atomic units. For visualizing the charge density within a 5 mRy energy window to the Fermi energy we used the atomic-sphere-approximation variant of the LMTO code [19].

In Fig. 1, we show the total and the  $l$ -resolved densities of states (DOS) of bcc yttrium. For comparison, we have also included the DOS for the hcp yttrium [12]. From Fig. 1, we see that the pressure-induced pushing out of  $s$ -electrons is followed by creation of new  $d$ -states between  $-0.55$  Ry and  $-0.25$  Ry to accommodate the  $s$ -electrons.

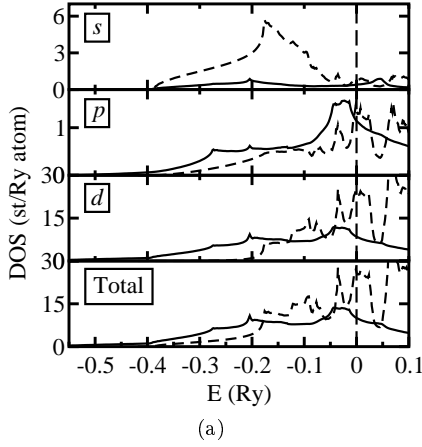


Figure 1: The  $s$ ,  $p$ ,  $d$  and the total densities of states of bcc (solid line) and hcp (dashed line) yttrium. The vertical dashed line indicates the Fermi energy.

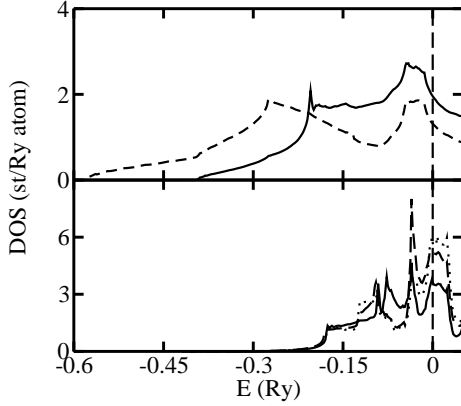


Figure 2: The symmetry-resolved  $d$  densities of states in bcc (top panel) and hcp (bottom panel) yttrium. The densities of states in the top panel correspond to  $t_{2g}$  ( $xy$ ,  $yz$  and  $zx$ ; solid line) and  $e_g$  ( $x^2 - y^2$  and  $3z^2 - 1$ ; dashed line) symmetries, while in the bottom panel they correspond to  $yz$  ( $zx$ ; solid line),  $xy$  ( $x^2 - y^2$ ; dashed line) and  $3z^2 - 1$  (dotted line) symmetries. The vertical dashed line indicates the Fermi energy.

The flattening of the  $d$ -band reduces the DOS at the Fermi energy to 10.03 st/Ry from its hcp value of 25.89 st/Ry, with most of the contributions coming from the  $d$ -states.

It is interesting to consider the symmetry-resolved  $d$ -DOS, as shown in Fig. 2. Some of the differences in the DOS between the ambient pressure hcp phase and the high-pressure bcc phase arise due to change in symmetry from hexagonal to cubic. In hcp phase, the three independent  $d$ -DOS corresponding to  $yz$  ( $zx$ ),  $xy$  ( $x^2 - y^2$ ) and  $3z^2 - 1$  symmetries have similar bandwidths but some differences in the DOS as a function of energy. However, in bcc phase the bottom of the doubly degenerate  $e_g$  ( $x^2 - y^2$  and  $3z^2 - 1$ ) symmetry DOS is almost 0.2 Ry below the bottom of the triply degenerate  $t_{2g}$  ( $xy$ ,  $yz$  and

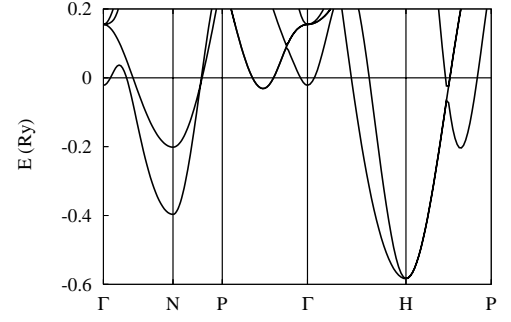


Figure 3: The band-structure of bcc yttrium (solid line) along high symmetry directions in the corresponding Brillouin zone. The horizontal line, passing through the energy zero, indicates the Fermi energy.

$zx$ ) symmetry DOS, indicating transfer of pushed-out  $s$ -electrons to  $e_g$  symmetry orbitals. A symmetry-resolved breakup of DOS at the Fermi energy is 0.40, 1.14, 5.87 and 2.62 st/Ry for  $s$ ,  $p$ ,  $t_{2g}$  and  $e_g$  symmetries, respectively.

As a prelude to understanding the Fermi surface topology and the nature of electrons contributing to the electron-phonon interaction, we show in Fig. 3, the calculated band-structure of bcc yttrium along high symmetry directions in the corresponding Brillouin zone. The band corresponding to  $4p$  state is much lower in energy, and hence it is not shown in the figure. Based on Fig. 3 and an analysis of the eigenvectors (not shown in the figure), the so-called fat bands, we find that the bands crossing the Fermi energy along  $\Gamma$ -N, N-P and H-P symmetry directions have substantial  $t_{2g}$  symmetry states, indicating an important role for these electrons as far as the electron-phonon interaction was concerned.

Since Fermi surface plays an important role in understanding many of the superconducting properties of materials, we show the calculated Fermi surface of bcc yttrium in Fig. 4. The Fermi surface due to band number 1 surrounds  $\Gamma$  point and it has a bucket-like structure around P symmetry point in the reciprocal space. The second band has an umbrella-like structure with four-fold symmetry around N point, in addition to having surfaces around  $\Gamma$  and P points. It turns out that some of the flat portions in all these surfaces lead to Fermi surface nesting especially along N-P and  $\Gamma$ -P symmetry directions, the indications of which can be seen in Figs. 4 (c) and (d), showing the Fermi surface cut in a plane parallel to (110) plane. A more detailed analysis is needed to clearly identify all the nesting vectors.

In Fig. 5 we show the charge density within a 5 mRy energy window around the Fermi energy in bcc yttrium, calculated using the tight-binding-LMTO method as mentioned earlier [19]. The  $e_g$  symmetry electrons seem to be localized around the yttrium sites while  $t_{2g}$  electrons are more spread out and hybridized with the nearby yttrium atoms. Having described the electronic

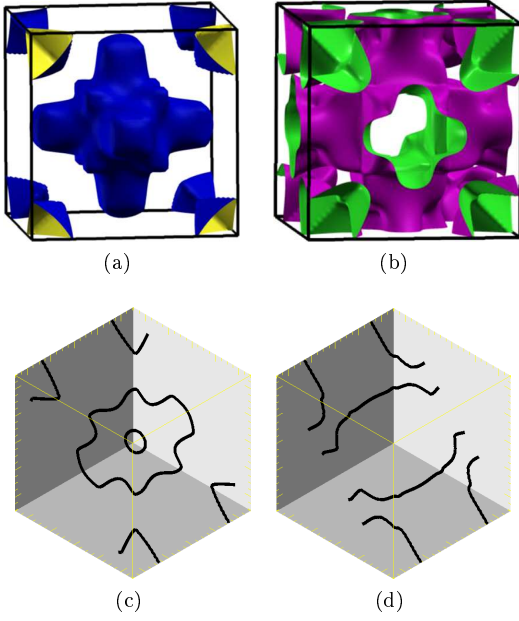


Figure 4: The Fermi surface of bcc yttrium in reciprocal space unit cell corresponding to (a) band number 1, and (b) band number 2. The Fermi surface cut on a plane parallel to (110) plane for (c) band number 1, and (d) band number 2. The center of the cube corresponds to the  $\Gamma$  point.

structure of bcc yttrium, we turn to its lattice-dynamical response and how the phonons couple to electrons close to Fermi energy.

Our calculated phonon density of states  $F(\omega)$  and the Eliashberg function  $\alpha^2F(\omega)$  of bcc yttrium are shown in Fig. 6, where we also show the corresponding values for hcp yttrium taken from our earlier work [12]. In the insets of Fig. 6, we show the variations of  $\omega$  and  $\lambda_{\mathbf{q}\nu}$  of bcc yttrium along  $\Gamma$ -N direction. A comparison of  $F(\omega)$  of bcc yttrium with that of hcp yttrium clearly shows the hardening of the bcc lattice, which has become almost three times as hard. Some of the significant additions to  $F(\omega)$  of bcc yttrium take place around the peak at 59 meV, the peak itself arising out of the displacement of yttrium atoms with components in all the three directions. We also find that the phonon mode (with displacement having components along  $+y$  and  $-z$  directions) in bcc yttrium along  $\Gamma$ -N direction softens to 9 meV at  $\mathbf{q} = (0.0, 0.375, 0.375)$  in units of  $2\pi/a$ , and it has a value of 12.6 meV at the N symmetry point. Phonon softening in fcc yttrium is discussed by Yin *et al.* [20].

The pressure-induced increase in  $\alpha^2F(\omega)$  in yttrium, accompanied by structural phase transformations, seems to arise from the enhancement of contributions from existing modes and coupling strongly to the newly created modes. For example, the peaks around 23 and 27 meV are created in the dhcp phase and they become much stronger in the bcc phase, while the peak at 59 meV is created in the bcc phase. As a result, the average

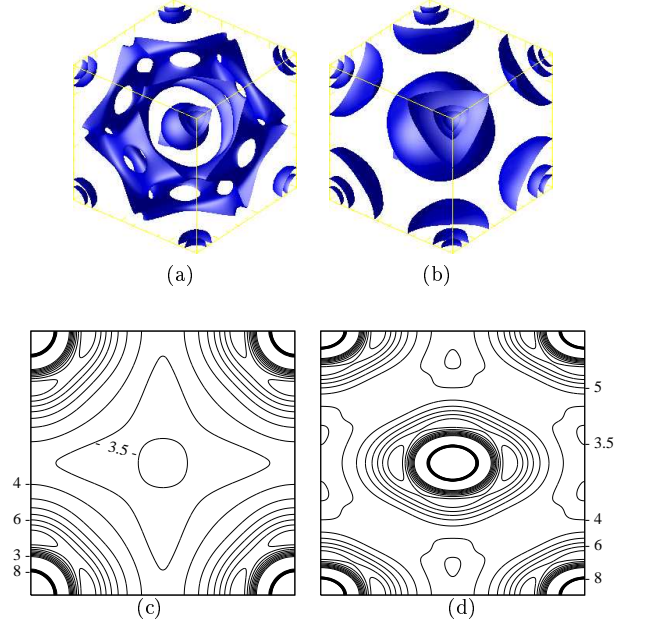


Figure 5: The isosurfaces and contours of charge density within a 5 mRy energy window around the Fermi energy in bcc yttrium. The values of the isosurfaces are (a) 3.5 and (b) 4.5 in units of  $10^{-2}[e/a.u.^3]$ , which is also the unit used in (c) and (d).

electron-phonon coupling constant  $\lambda$  increases from 0.46 in hcp yttrium to 1.8 in bcc yttrium.

Somewhat surprisingly, we find that the largest contribution of  $\lambda_{\mathbf{q}\nu} \approx 5$  to  $\lambda_{\mathbf{q}} = 5.9$  comes from the phonon mode along  $\Gamma$ -N direction with  $\mathbf{q}$  as mentioned above. At N symmetry point, the same mode contributes  $\lambda_{\mathbf{q}\nu} \approx 2.9$  to  $\lambda_{\mathbf{q}} = 5.2$ . Smaller contributions with  $\lambda_{\mathbf{q}\nu} > 1$  also come from  $\mathbf{q}$ -points lying close to  $\Gamma$ -P direction and towards H point. The fact that the smaller regions in reciprocal space make substantial contributions to the electron-phonon coupling, a precise determination of  $\lambda$  using a uniform  $\mathbf{q}$ -grid becomes computationally difficult. Since most of these contributions come from the low energy phonons, it is not expected to have a significant effect on the determination of  $T_c$ . To illustrate the point, we also show in Fig. 6, the  $F(\omega)$  and  $\alpha^2F(\omega)$  of bcc yttrium calculated at the lattice constant  $a = 5.1987$  a.u. as described earlier. Not surprisingly, the difference in  $\lambda$ , resulting from the two sets of calculations, is more pronounced in 15-25 meV region.

The most important result of the present work is obtained by solving numerically the isotropic gap equation [16, 17] using the calculated Eliashberg function  $\alpha^2F(\omega)$ . The results of such a calculation for bcc yttrium as a function of  $\mu^*$  is shown in Fig. 7. We find that for  $\mu^*$  ranging from 0.1 to 0.25, the  $T_c$  values range from 47.7 to 36.8 K. A comparison of our calculated  $T_c$ , including the ones described in Ref. [12], with experiment is shown in Fig. 7. Thus, the present work clearly shows

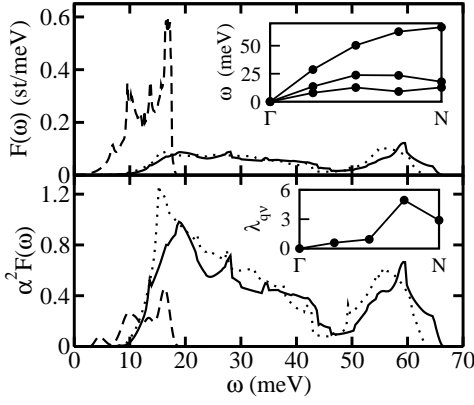


Figure 6: The phonon density of states  $F(\omega)$  (top panel) and the Eliashberg function  $\alpha^2 F(\omega)$  (bottom panel) of bcc (solid line) and hcp (dashed line) yttrium. The dotted line in the two panels show  $F(\omega)$  and  $\alpha^2 F(\omega)$  of bcc yttrium at  $a = 5.1987$  a.u., respectively. The two insets show  $\omega$  and  $\lambda_{qv}$  (for the lowest mode) along  $\Gamma$ -N direction. In the top panel, the phonon density of states of hcp yttrium has been reduced by a factor of 4 for clarity.

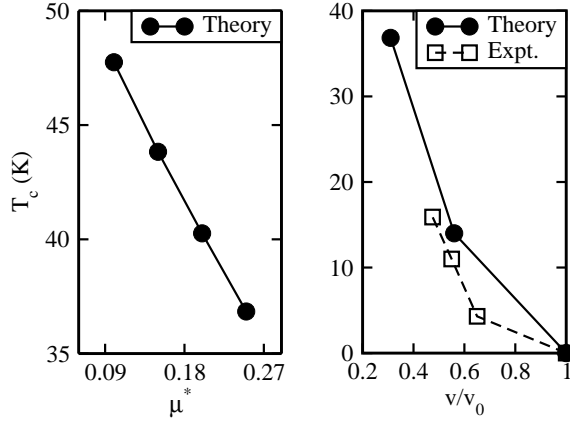


Figure 7: The calculated  $T_c$  (solid circles) as a function of  $\mu^*$  (left panel) and  $v/v_0$  (right panel). Experimentally observed  $T_c$  (open squares), taken from Ref. [1], are also shown in the right panel. The calculated  $T_c$  for hcp and dhcp phases of yttrium are taken from Ref. [12].

the possibility of a  $T_c$  of 30 K or above for compressed, bcc yttrium.

In conclusion, we have shown that compressed, bcc

yttrium has a large electron-phonon coupling with  $\lambda = 1.8$ , leading to a superconducting transition temperature  $T_c \approx 30$  K or above. We have also shown that such a large coupling is a direct consequence of lattice hardening and its subsequent coupling to Fermi electrons.

\* Electronic address: ppsingh@phy.iitb.ac.in

- [1] J. J. Hamlin, V. G. Tissen, and J. S. Schilling, Phys. Rev. B **73**, 094522 (2006).
- [2] W. A. Grosshans and W. B. Holzapfel, Phys. Rev. B. **45**, 5171 (1992).
- [3] Y. K. Vohra, H. Olijink, W. Grosshans, and W. P. Holzapfel, Phys. Rev. Lett. **47**, 1065 (1981).
- [4] C. Probst and J. Wittig, in *Handbook on the Physics and Chemistry of Rare Earths*, edited by J. K. A. Gschneidner and L. Eyring (North-Holland, Amsterdam, 1978), p. 749.
- [5] M. Hanfland, K. Syassen, N. E. Christensen, and D. L. Novikov, Nature (London) **408**, 174 (2000).
- [6] N. W. Ashcroft, Nature (London) **419**, 569 (2002).
- [7] J. Melsen, J. M. Wills, B. Johansson, and O. Eriksson, Phys. Rev. B. **48**, 15574 (1993).
- [8] K. Shimizu, H. Kimura, D. Takao, and K. Amaya, Nature **419**, 597 (2002).
- [9] V. V. Struzhkin, M. I. Erements, W. Gan, H.-K. Mao, and R. J. Hemely, Science **298**, 1213 (2002).
- [10] G. Profeta, C. Franchini, N. N. Lathiotakis, A. Floris, A. Sanna, M. A. L. Marques, M. Luders, S. Massidda, E. K. U. Gross, and A. Continenza, Phys. Rev. Lett. **96**, 047004 (2006).
- [11] D. Kasinathan, J. Kunes, A. Lazicki, H. Rosner, C. S. Yoo, R. T. Scalettar, and W. E. Pickett, Phys. Rev. Lett. **96**, 047004 (2006).
- [12] P. P. Singh, cond-mat/0607176.
- [13] S. Y. Savrasov, Phys. Rev. B **54**, 16470 (1996).
- [14] S. Y. Savrasov and D. Y. Savrasov, Phys. Rev. B **54**, 16487 (1996).
- [15] P. B. Allen and R. C. Dynes, Phys. Rev. B **12**, 905 (1975).
- [16] P. Allen and B. Mitrovic, in *Advances in Solid State Physics*, edited by H. Ehrenreich, F. Seitz, and E. Turnbull (Academic Press, New York, 1982), 37, p. 1.
- [17] P. B. Allen, private communication.
- [18] *xcrysden code*; <http://www.xcrysden.org/>.
- [19] *Stuttgart tb-lmto code*.
- [20] Z. P. Yin, S. Y. Savrasov, and W. E. Pickett, cond-mat/0606538.